6th June 2014

Cysteine-Cystine Redox Cycling in a Gold-Gold Dual-Plate Generator-Collector Microtrench Sensor

Jules L. Hammond [a], Andrew J. Gross [b], Pedro Estrela [a], Jesus Iniesta [c], Stephen J. Green [d], C. Peter Winlove [d], Paul G. Winyard [e], Nigel Benjamin [e], and Frank Marken [b]

[a] *Department of Electronic & Electrical Engineering, University of Bath, Bath BA2 7AY, UK*
[b] *Department of Chemistry, University of Bath, Bath BA2 7AY UK*
[c] *Universidad Alicante, Department of Physical Chemistry and Institute for Electrochemistry, 03080 Alicante, Spain*
[d] *Department of Physics, College of Engineering, Mathematics and Physical Sciences, University of Exeter, Stocker Road, Exeter EX4 4QL, UK*
[e] *University of Exeter Medical School, University of Exeter, St Luke's Campus, Exeter, EX1 2LU, UK*

To be communicated to Analytical Chemistry

F.Marken@bath.ac.uk

Abstract

Thiols and disulfides are ubiquitous and important analytical targets. However, their redox properties, in particular on gold sensor electrodes, are complex and obscured by strong adsorption. Here, a gold-gold dual-plate micro-trench dual-electrode sensor with feedback signal amplification is demonstrated to give well-defined (but kinetically limited) steady-state voltammetric current responses for the cysteine-cystine redox cycle in non-degassed aqueous buffer media at pH 7 down to micro-molar concentration levels.

Keywords: *electroanalysis, gold electrodes, thiol, protein, sensors, voltammetry, junctions, water analysis.*

Introduction

Cysteine is an α-amino acid found in many natural proteins and physiological media. Cystine, the oxidized dimer of cysteine provides a modality for the crosslinking through disulfide bonds, important in defining the primary, secondary and tertiary structure of proteins. The sulfhydryl group in cysteine is partially deprotonated at physiological pH, enhancing reactivity and allowing the formation of reversible oxidative post-translational modifications (oxPTMs) that act as a signalling mechanism, regulating protein function, interaction and localization [1,2]. *In vivo*, thiol-disulfide redox cycling is catalyzed by thiol oxidases and disulfide reductases in the endoplasmic reticulum and periplasmic space [3]. Typical concentrations of L-cysteine in blood plasma are between 200 to 300 μM and can be useful as a medical indicator in human diseases involving abnormal cysteine metabolism [4].

The electrochemical detection of the cysteine/cystine redox couple offers advantages of being more affordable and miniaturizable, as well as providing fast and sensitive detection when compared to spectrometric [5] or chromatography [6] techniques. However, in particular for thiols and disulfides very few analytical procedures have been developed due to the complexity of these redox systems. The oxidation of cysteine has been investigated on different types of electrodes [7,8,9] and found to proceed (depending on electrode material and applied potential) via multi-electron pathway producing cysteic acid (6 electrons) as final product with further complications due to strong thiol adsorption on metal surfaces. The one-electron

product, cystine, also is strongly adsorbed and requires highly negative applied potential for reductive desorption back to cysteine [10]. A new method to overcome this chemical complexity can be based on generator-collector sensors [11].

Advantages of amplification by generator-collector feedback have been pioneered and exploited for example by Christensen [12], by Hubbard [13], and by Seddon [14]. More recently Lemay has demonstrated nano-scale generator-collector electrode systems with extreme sensitivity down to the single molecule level [15,16,17]. Pulse methods were reported for glucose detection in a gold-gold dual-hemisphere electrode system with nano-gap [18]. Microtrench or dual-plate electrodes with inter-electrode gap of typically 2 to 80 μm and an aspect ratio of typically 10 have been developed to allow for example dopamine detection [19], pH titration [20], and liquid-liquid anion transfer detection [21]. The benefits of this dual-plate electrode geometry are (i) rapid and mostly planar inter-electrode diffusion within the trench, (ii) rapid diffusion of analyte into the trench, (iii) discrimination of chemically reversible targets from irreversible interferences (e.g. oxygen or ascorbate), and (iv) improved specificity from two applied electrode potentials. In this report a gold-gold dual-plate microtrench sensor is employed for the detection of cysteine/cystine.

Figure 1A shows a schematic depiction of the simplified reaction scheme with the redox system cysteine/cystine represented by Red/Ox. The gold-gold dual-plate microtrench electrode employed here should allow steady state current responses to be obtained irrespective of the complexity in the reaction scheme and with potential for future analytical applications.

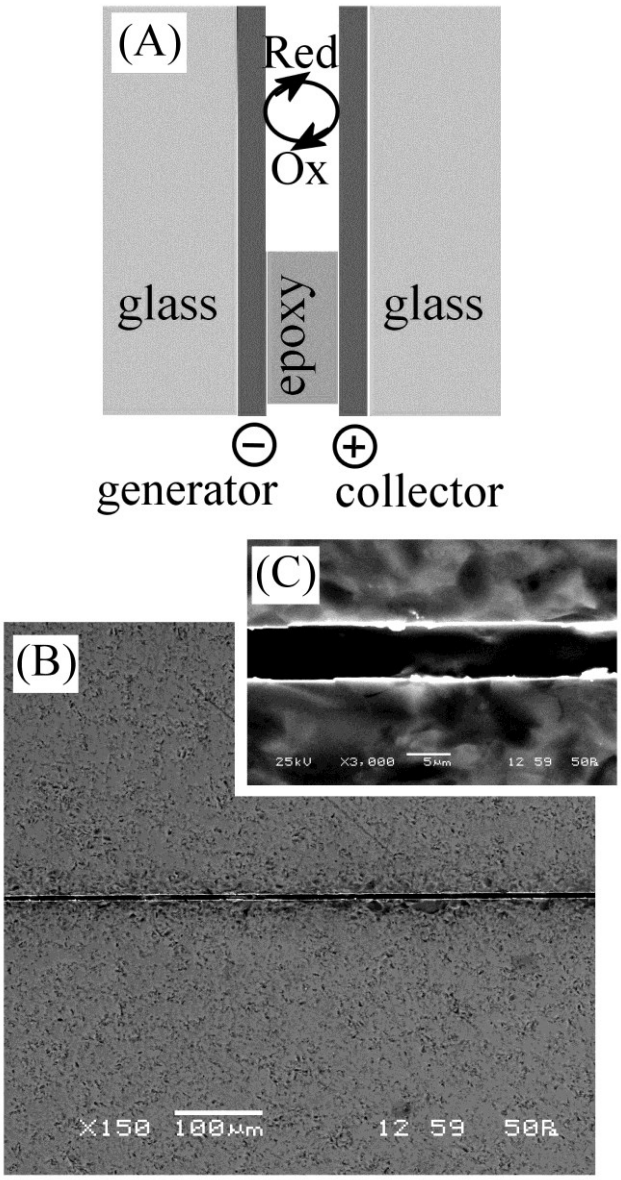

Figure 1. (A) Schematic drawing of the micro-trench sensor in feedback mode. (B,C) SEM images of the gold-gold dual-plate microtrench with ca. 6 μm width.

Experimental

Reagents

L-cysteine (97%), L-cystine (99%), sodium hydroxide (98-100.5%), sodium phosphate monobasic (98-102%), and potassium chloride (99-100.5%) were purchased from Sigma-Aldrich and used without further purification. Purified water (18.2 MΩ cm) from a PURELAB Classic purifier (ELGA) was used to make solutions. L-cysteine was stored below 5°C and both L-cysteine and L-cystine solutions were prepared immediately before use with 1 minute sonication to assist solubilization.

Instrumentation

Electrochemical measurements were performed using an Autolab PGSTAT12 (Metrohm) bi-potentiostat equipped with a differential electrometer amplifier. A four-electrode arrangement was utilised, comprised of a saturated KCl calomel electrode (SCE, Radiometer REF 401), platinum wire counter electrode, and the two working electrodes of the gold-gold microtrench electrode. In some experiments a conventional 1 mm diameter gold disc working electrode was employed in a three-electrode arrangement. A Teflon® jig was used to hold the four electrodes in place within a 50 mL glass beaker. GPES software was used to perform cyclic voltammetry at the generator whilst holding the collector electrode at a constant voltage. Linear baseline correction within GPES was used to improve presentation of data where appropriate. SEM images were taken with a SEM6480LV microscope (JEOL).

Procedure: Growth of Gold-Gold Junction Electrodes

Figure 1B and 1C show SEM images of the microtrench electrode with ca. 6 μm inter-electrode gap. This type of electrode has a depth of ca. 60 μm (aspect ratio 10; determined by electrochemical calibration with a $Fe(CN)_6^{3-/4-}$ redox system [20]). The fabrication was based on 100 nm gold-coated microscope slides (Sigma-Aldrich), which were sliced into 10 mm x 25 mm strips using a diamond cutter (Buehler Isomet 1000). A central 5 mm x 25 mm region of a strip was masked using Kapton® tape before etching the exposed gold for 3 minutes using aqua regia (1:3 nitric acid : hydrochloric acid; *warning: this solution is highly corrosive*). The etching process was stopped by rinsing with water. In order to oxidise the remaining titanium adhesion layer the electrodes were placed into a furnace at 500°C for 30 minutes. Epoxy (Gurit SP106) was used to bond two opposing electrodes, with the epoxy given 1 hour to pre-cure before application of pressure. The base of the micro-trench was sliced off using a diamond cutter and polished using decreasing grits of SiC abrasive paper (Buehler). Finally, the epoxy was etched out using piranha solution (5:1 sulphuric acid : hydrogen peroxide; *warning: this solution is highly corrosive*) to form the trench.

Results and Discussion

Cysteine-Cystine Redox Processes at Gold Electrodes

The oxidation of cysteine is known to occur in a complex multi-electron process via cystine to give products including cysteic acid [22,23], in particular in alkaline media. However, when performed under controlled potential conditions and at neutral pH, the one-electron oxidation per cysteine to cystine should be observed (equation 1).

$$2\ \text{cysteine (aq)} \rightleftharpoons \text{cystine (aq)} + 2H^+ + 2\ e^- \qquad (1)$$

On gold electrodes further processes are expected due to effective adsorption of thiols and disulfides to the surface and due to the well-known gold surface oxidation in aqueous phosphate buffer at pH 7 [24]. Figure 2A shows typical cyclic voltammograms with (i) a background response consistent with gold and (ii) a clear oxidation peak at 0.6 V vs. SCE similar for example to that reported for N-acetyl-cysteine [25]. The peak current of ca. 22 μA allows the apparent diffusion coefficient for cysteine to be estimated based on the Randles-Sevcik equation, which is employed here only to provide an approximate bench mark value for the diffusion limited peak current (equation 2).

$$I_p = 0.446 \times nFAc\sqrt{\frac{nFvD}{RT}} \qquad (2)$$

In this equation I_p is the peak current, n = 1 is assumed for cystine formation (*vide infra*), F is the Faraday constant, v is the potential scan rate, R is the gas constant, T is

the absolute temperature, and the apparent diffusion coefficient D can then be obtained as 6×10^{-9} m^2s^{-1}. This value is much too high to be physically realistic (the literature value is $D_{cysteine} = 0.81 \times 10^{-9}$ m^2s^{-1} [26]) and therefore an indication of either (i) multi-electron transfer or (ii) contributions from adsorbed cysteine, or both. It is known that cysteine strongly adsorbs onto gold electrode prior to oxidation [27].

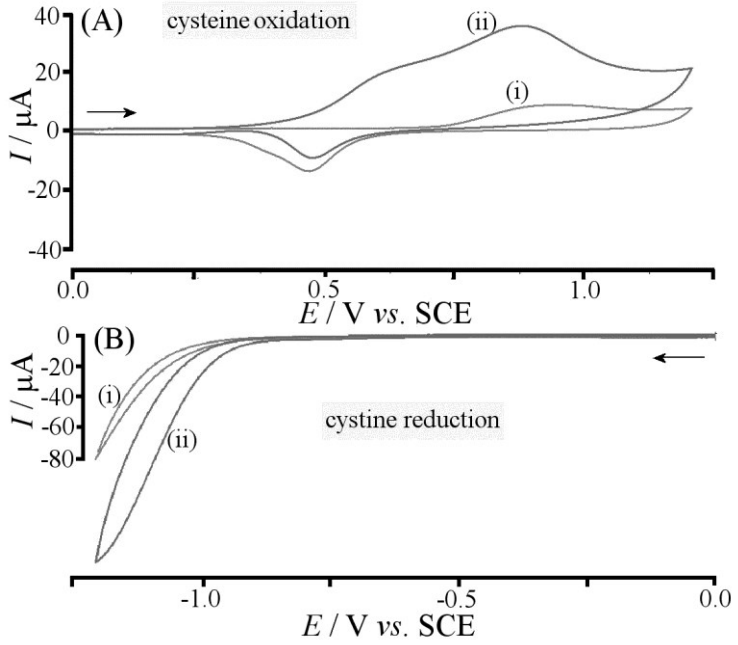

Figure 2. Cyclic voltammograms (scan rate 0.1 Vs^{-1}, 1 mm diameter gold disc electrode, 0.1 M phosphate buffer pH 7) for (A) the oxidation of 1 mM cysteine and (B) the reduction of 1 mM cystine. The trace (i) shows the background signal without analyte.

The back-reduction of cystine to cysteine formally is a 2-electron process (see equation 1) and has been reported previously, for example on Pb electrodes [28]. The diffusion coefficient was determined as $D_{cystine} = 0.48 \times 10^{-9}$ m^2s^{-1}. Data in Figure 2B suggest that there is a cystine reduction at the gold electrode surface commencing at -0.8 V vs. SCE but without clear peak feature and with a quite high current (ca. 40 μA

at -1.2 V *vs*. SCE), therefore again affected by adsorption of cystine on the electrode. In addition to the reduction response for cystine, an oxidation response similar to that observed for cysteine at 0.6 V vs. SCE (not shown) is observed, indicative of more complexity involving surface-adsorbed intermediates and/or multi-electron oxidation or cystine to cysteic acid. Given the complexity observed for cysteine/cystine at single gold electrodes, it is interesting to explore reactivity at Au-Au dual-plate generator-collector electrode systems. The observation of a cysteine/cystine redox cycle would offer a way to distinguish the well-defined redox cycle from more complex redox and background processes.

Generator-Collector Processes I.: Oxidation of Cysteine

Initial experiments at the Au-Au generator-collector microtrench electrode were performed with the generator scanning into the cysteine oxidation and the collector at fixed potential. Figure 3A shows that there was indeed a feedback current with the collector potential held sufficiently negative, here -0.5 V vs. SCE, with good responses being recorded at $E_{collector}$ = -0.85 V vs. SCE. Next, the cysteine concentration was varied (see Figure 3B) and the plot of collector current versus concentration shows reasonable linearity, consistent with a generator-collector feedback process (see Figure 3C). In spite of the complexity of the overall redox process, a feedback current can be identified tentatively (assuming mass transport control) expressed in terms of the Nernst model for dual-plate diffusion processes [20] as

$$I_{\lim,diffusion} = \frac{2FAc_0}{\delta} \frac{D_{cysteine} \times D_{cystine}}{D_{cysteine} + D_{cystine}} \quad (3)$$

In this equation $I_{\lim,diffusion}$ is the microtrench feedback current under mass transport control, F and A are the Faraday constant and electrode area, δ = 6 μm is the inter-electrode gap, and the concentration is defined as $c_0 = 2\ c_{cystine} + c_{cysteine}$. Based on this expression, and with a 60 μm trench depth, the predicted slope for the plot in Figure 3C is 2.9 μA mM^{-1}, which is 20 times higher than that observed experimentally. Therefore the feedback current appears to be inconsistent with diffusion control and more likely to be kinetically limited (*vide infra*).

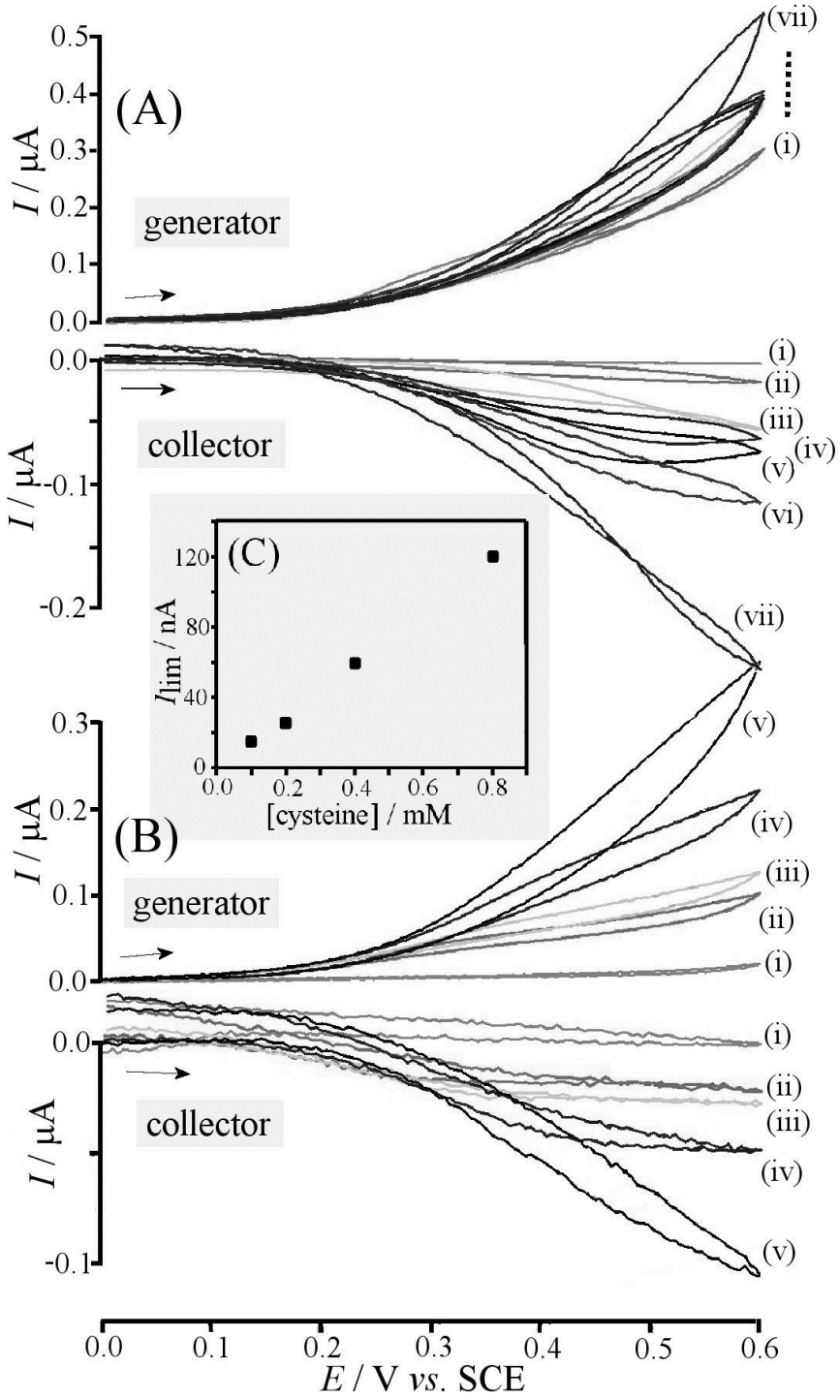

Figure 3. Generator-collector voltammograms (scan rate 0.025 Vs^{-1}, gold-gold dual-plate micro-trench, 0.1 M phosphate buffer pH 7) for the oxidation and back-reduction of 1 mM cysteine. (A) Data obtained with collector potentials (i) -0.25, (ii) -0.45, (iii) -0.55, (iv) -0.65, (v) -0.75, (vi) -0.85, (vii) -0.95 V vs. SCE. (B) Data obtained with collector potential -0.85 and (i) 0, (ii) 0.1, (iii) 0.2, (iv) 0.4, (v) 0.8 mM cysteine. (C) Plot of limiting current versus concentration of cysteine.

Generator-Collector Processes II.: Reduction of Cystine

The cystine reduction at the Au-Au microtrench is mechanistically equivalent to the case of cysteine oxidation (the same coupled redox chemistry occurs with generator and collector switching roles, see equation 1). Voltammetric data in Figure 4A show the onset of the collector response with the collector potential set to 0.4 V vs. SCE with good feedback currents observed with collector potential 0.6 V vs. SCE. An offset current in the collector response is indicative of some additional oxidation (possibly multi-electron thiol oxidation) at this potential. A current step in the generator signal at -0.4 V vs. SCE shows a weak oxygen reduction (solutions were not de-aerated) without significant effect on the collector response.

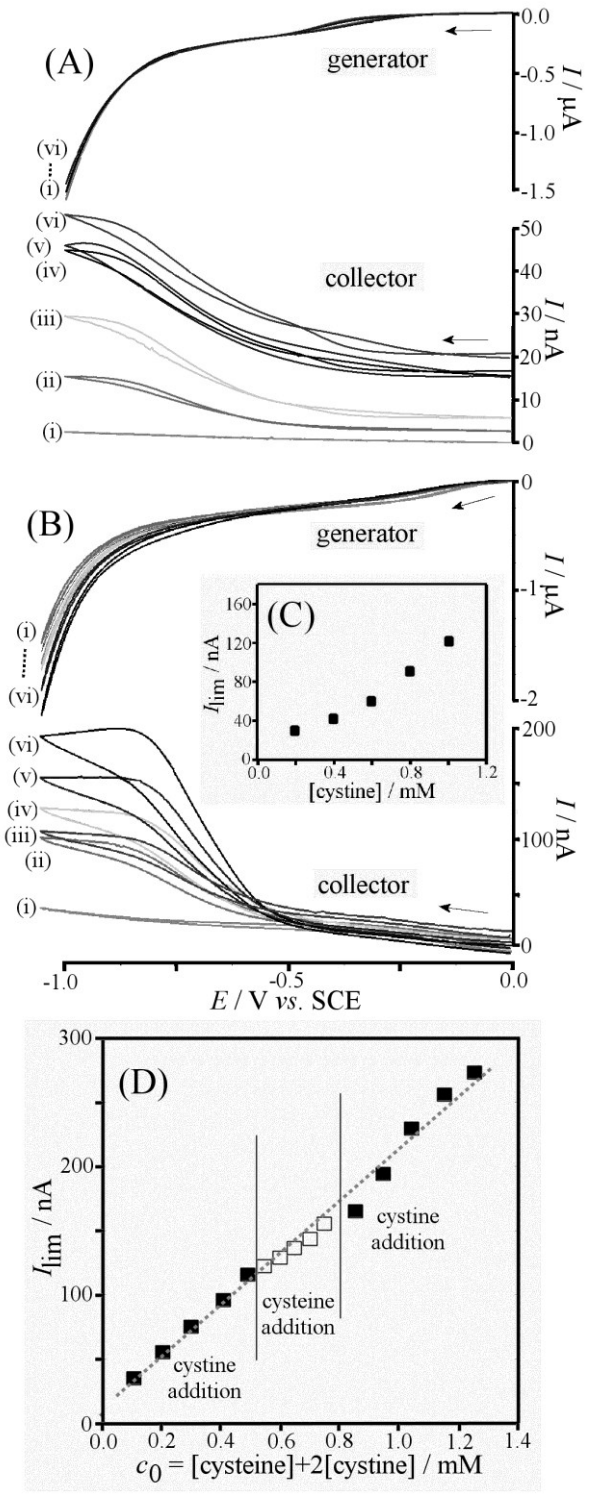

Figure 4. Generator-collector voltammograms (scan rate 0.025 Vs^{-1}, gold-gold dual-plate micro-trench, 0.1 M phosphate buffer pH 7) for the reduction and back-oxidation of 1 mM cystine. (A) Data obtained with collector potentials (i) 0.15, (ii) 0.35, (iii) 0.55, (iv) 0.60, (v) 0.65, (vi) 0.70 V vs. SCE (data shifted along current axis to overlay). (B) Data obtained with collector potential 0.60 and (i) 0, (ii) 0.2, (iii) 0.4, (iv) 0.6, (v) 0.8, (vi) 1.0 mM cystine. (C) Plot of limiting current versus concentration of cystine. (D) Plot for limiting current versus c_0 for sequential 50 μM addition of both cysteine and cystine.

When varying the cystine concentration (with 0.6 V vs. SCE collector potential), a well-defined feedback current is detected at -0.8 V vs. SCE generator potential (Figure 4B) and a plot of the observed current versus cystine concentration (Figure 4C) suggests approximately linear correlation. The current-concentration slope observed experimentally again an order of magnitude lower than that expected based on equation 3. Therefore simple diffusion controlled reaction conditions are unlikely to govern this process. It is possible to express the case of a kinetically limited microtrench process based on $I_{ox} = FA\ k_{ox}$ [cysteine] and $I_{red} = 2FA\ k_{red}$ [cystine]. Irrespective of the nature of k_{ox} and k_{red}, equating these two expressions shows that [cystine]/[cysteine] = $k_{ox}/2k_{red}$, which suggests that depending on the applied potential either cystine or cysteine will be present in the microtrench. Substitution with c_0 = [cysteine] + 2[cystine] then gives the microtrench limiting current as

$$I_{\lim,kinetic} = FAc_0 \frac{k_{ox} \times k_{red}}{k_{ox} + k_{red}} \qquad (4)$$

A kinetically controlled limiting current should be obtained linear in c_0. This is demonstrated in Figure 4D for sequential 50 μM additions of cystine and cysteine. The agreement with equation 4 is acceptable and remaining non-linearity may be associated with the adsorption/desorption kinetics, some degree of multi-electron oxidation, and the transient nature of the cyclic voltammetry experiment. Effects of adsorption kinetics, in particular in nanogap sensors, have been discussed recently by Mathwig and Lemay [29].

It is interesting to note that all experiments here were conducted in the presence of ambient levels of oxygen. The reduction of oxygen is observed at the generator at -0.4 V vs. SCE (see Figure 4A), but this appears not to interfere with the cysteine/cystine redox signal. For the overall cysteine/cystine process there are two possible scenarios to explain the lower than diffusion-limited current responses:

(A) If the cysteine oxidation occurs as a multi-electron process with products other than cystine, this will induce a concentration depletion effect within the microtrench.

(B) If a slow surface process is associated with a kinetically limiting factor (most likely slow electron transfer associated with adsorption/desorption), lower conversion and therefore lower currents would be expected during feedback across the microtrench.

The second hypothesis appears to be most likely here, but the first process may also contribute significantly. In future, further experiments are required with either a mesoporous gold electrode surface (to overcome slow surface processes with high surface area [30]) or a significantly smaller inter-electrode gap (to overcome/outrun multi-electron transfer depletion effects). Other electrode materials and/or electrocatalysts could be introduced to provide “fingerprint” information on different types of thiols and disulfides.

Conclusion

It has been demonstrated that even for complex analytical systems such as cysteine/cystine on gold at pH 7 and in the presence of air, dual-plate generator-collector electrode systems allow analytically useful current responses to be obtained. Interfering current signals such as those from gold surface oxidation and/or thiol adsorption are suppressed and the analytical signal of interest is feedback-enhanced. For both processes - cysteine oxidation and cystine reduction - similar behaviour and similar sensitivity were observed in accordance with the equivalence of both in the overall microtrench redox cycle. It is likely that some anodic over-oxidation of cysteine is a factor here in suppressing the analytical signal due to depletion of analyte within the microtrench. Even more important is probably the kinetic limitation inherent in cysteine oxidation and in cystine reduction when adsorbed on gold. In future, sub-micrometer "nano-trench" electrode systems based on appropriate or better electrode materials may allow short-lived intermediates such as the cysteine radical to be "caught" and redox-recycled more effectively. Sensing applications are feasible for a wider range of thiols and under physiological conditions.

Acknowledgements

J.L.H. is supported by an UK Engineering and Physical Sciences Research Council (EPSRC) Doctoral Training Award. A.J.G. and F.M. gratefully acknowledge EPSRC funding (EP/I028706/1).

References

(1) Paulsen, C.; Carroll, K., Chem. Rev., **2013**, *113*, 4633-4679.

(2) Winyard, P.G.; Moody, C.J.; Jacob, C., Trends Biochem. Sci., **2005**, *30*, 453-461.

(3) Sevier, C.; Kaiser, C., Nature Rev. Mol. Cell Biol., **2002**, *3*, 836-847.

(4) Salemi, G.; Gueli, M.; D'Amelio, M.; Saia, V.; Mangiapane, P.; Aridon, P.; Ragonese, P.; Lupo, I., Neurol. Sci., **2009**, *30*, 361-364.

(5) Hao, W.H.; McBride, A.; McBride, S,; Gao, J.P.; Wang, Z.Y., J. Mater. Chem., **2011**, *21*, 1040–1048.

(6) Guan, X.; Hoffman, B.; Dwivedi, C.; Matthees, D.P., J. Pharm. Biomed. Anal., **2003**, *31*, 251–261.

(7) Ralph, T.R.; Hitchman, M.L.; Millington, J.P.; Walsh, F.C., J. Electroanal. Chem., **1994**, *375*, 1-15.

(8) Lai, Y.T.; Ganguly, A.; Chen, L.C.; Chen, K.H., Biosens. Bioelectronics, **2010**, *26*, 1688-1691.

(9) Shaidarova, L.G.; Ziganshina, S.A.; Gedmina, A.V.; Chelnokova, I.A.; Budnikov, G.K., J. Anal. Chem., **2011**, *66*, 633-641.

(10) Wang, C.Y.; Liu, Q.X.; Shao, X.Q.; Hu, X.Y., Anal. Lett. **2007**, *40*, 689-704.

(11) Barnes, E.O.; Lewis, G.E.M.; Dale, S.E.C.; Marken, F.; Compton, R.G., Analyst, **2012**, *137*, 1068-1081.

(12) Christensen, C.R.; Anson, F.C., Anal. Chem., **1963**, *35*, 205-209.

(13) Hubbard, A.T.; Peters, D.G., CRC Crit. Rev. Anal. Chem. **1973**, *3*, 201-242.

(14) Seddon, B.J.; Wang, C.F.; Peng, W.F.; Zhang, X.J., J. Chem. Soc., Faraday Trans., **1994**, *90*, 605-608.

(15) Katelhon, E.; Hofmann, B.; Lemay, S. G.; Zevenbergen, M. A. G.; Offenhausser, A.; Wolfrum, B., Anal. Chem., **2010**, *82*, 8502-8509.

(16) Zevenbergen, M.A.G.; Singh, P.S.; Goluch, E.D.; Wolfrum, B.L.; Lemay, S.G., Nano Lett. **2011**, *11*, 2881-2886.

(17) Kang, S.; Nieuwenhuis, A.; Mathwig, K.; Mampallil, D.; Lemay, S.G., ACS

Nano, **2013**, *7*, 10931-10937.

(18) Rassaei, L.; Marken, F., Anal. Chem., **2010**, *82*, 7063-7067.

(19) Hasnat, M.A.; Gross, A.J.; Dale, S. E. C.; Barnes, E. O.; Compton, R. G; Marken, F., Analyst, **2013**, *139*, 569-575.

(20) Dale, S.E.C.; Vuorema, A.; Sillanpää, M.; Weber, J.; Wain, A.J.; Barnes, E.O.; Compton, R.G.; Marken, F. Electrochim. Acta, **2014**, *125*, 94-100.

(21) Dale, S. E C; Chan, Y.; Bulman Page, P. C; Barnes, E. O; Compton, R. G; Marken, F., Electrophoresis, **2013**, *34*, 1979-1984.

(22) Sires, I.; Delucchi, M.; Panizza, M.; Ricotti, R.; Cerisola, G., J. Appl. Electrochem., **2009**, *39*, 2275-2284.

(23) Enache, T.A.; Oliveira-Brett, A.M., Bioelectrochem., **2011**, *81*, 46-52.

(24) Milsom, E.V.; Novak, J.; Oyama, M.; Marken, F., Electrochem. Commun., **2007**, *9*, 436-442.

(25) Barus, C.; Gros, P.; Comtat, M.; Daunes-Marion, S.; Tarroux, R., Electrochim. Acta, **2007**, *52*, 7978-7985.

(26) Abbaspour, A.; Ghaffarinejad, A., Electrochim. Acta, **2008**, *53*, 6643-6650.

(27) Uvdal, K.; Bodo, P.; Liedberg, B., J. Coll. Interface Sci., **1992**, *149*, 162-173.

(28) Ralph, T.R.; Hitchman, M.L.; Millington, J.P.; Walsh, F.C., J. Electroanal. Chem., **2005**, *583*, 260-272.

(29) Mathwig, K.; Lemay, S.G., Electrochim. Acta, **2013**, *112*, 943-949.

(30) Liu, Z.; Zhang, H.C.; Hou, S.F.; Ma, H., Microchim. Acta, **2012**, *177*, 427-433.